NJC

PAPER

View Article Online
View Journal

Application of an indenyl molybdenum dicarbonyl complex in the isomerisation of α-pinene oxide to campholenic aldehyde†

Cite this: DOI: 10.1039/c4nj00371c

Sofia M. Bruno,[a] Ana C. Gomes,[a] Carla A. Gamelas,[bc] Marta Abrantes,[d] M. Conceição Oliveira,[d] Anabela A. Valente,*[a] Filipe A. Almeida Paz,[a] Martyn Pillinger,[a] Carlos C. Romão[b] and Isabel S. Gonçalves*[a]

Received (in Porto Alegre, Brazil) 12th March 2014,
Accepted 15th April 2014

DOI: 10.1039/c4nj00371c

www.rsc.org/njc

The complex $[\{(\eta^5\text{-Ind})Mo(CO)_2(\mu\text{-Cl})\}_2]$ (**1**) has been tested for the industrially relevant catalytic isomerisation of α-pinene oxide (PinOx) to campholenic aldehyde (CPA) in the liquid phase. PinOx conversion and CPA selectivity are strongly influenced by the solvent employed. Complete conversion of PinOx was achieved within 1 min at 55 °C or 30 min at 35 °C using 1,2-dichloroethane as solvent, giving CPA in 68% yield. Other products included *trans*-carveol, iso-pinocamphone and *trans*-pinocarveol. The stability of **1** under the reaction conditions used was investigated by using FT-IR spectroscopy and electrospray ionisation mass spectrometry (ESI-MS) to characterise recovered solids. In the presence of air/moisture **1** undergoes oxidative decarbonylation upon dissolution to give oxomolybdenum species that are proposed to include a tetranuclear oxomolybdenum(v) complex. Conversely, ESI-MS studies of **1** dissolved in dry acetonitrile show mononuclear species of the type $[IndMo(CO)_2(CH_3CN)_n]^+$. The crystal structure of the ring-slipped dicarbonyl complex $[(\eta^3\text{-Ind})Mo(CO)_2Cl(CH_3CN)_2]$ (**2**) (obtained after dissolution of **1** in acetonitrile) is reported.

Introduction

Food, flavor, fragrance, cosmetics and pharmaceutical industries make use of terpenes as feedstocks.[1] In particular, α-pinene is a monoterpene present in turpentine oil extracts of some coniferous trees, *e.g.* pine tree.[2] The epoxidation of α-pinene (Pin) gives α-pinene oxide (PinOx) which in turn can undergo acid-catalysed rearrangements to give a variety of value-added products of commercial interest,[3] *e.g.* campholenic aldehyde (CPA), *trans*-carveol, *trans*-sobrerol, pinocarveol, iso-pinocamphol, iso-pinocamphone,[4–6] among others.[2–7] In particular CPA is used in the manufacture of commercial sandalwood-like fragrances, *e.g.* Sandalore® and Javanol® (Givaudan), Bacdanol® (IFF), Brahmanol® (Dragoso) and Polysantol® (Firmenich).[8]

Different types of catalysts have been tested for this reaction, including transition metal salts and Keggin-type heteropolyacids.[2,4,9–12] We recently explored organometallic complexes for the catalytic isomerisation of PinOx to CPA, and interesting results were obtained in the case of $[(\eta^5\text{-Ind})Mo(\eta^3\text{-}C_3H_5)(CO)_2]$ (Ind = indenyl, C_9H_7; 56% CPA yield at 97% PinOx conversion, 3 h reaction at 35 °C).[13] Indenyl molybdenum compounds are of special interest due to the tendency of the indenyl ligand to undergo ring-slippage induced by electrochemical reduction or ligand addition. This hapto-flexibility allows enhancement of the reaction rates of substitution reactions of electronically saturated indenyl metal complexes, relative to their cyclopentadienyl congeners, finding application in some important organic reactions.[14] To the best of our knowledge, the use of indenyl molybdenum dicarbonyl complexes for homogeneous catalytic reactions has so far been restricted to the aforementioned study.[13] In contrast, cyclopentadienyl molybdenum dicarbonyl complexes are far more explored, particularly as precatalysts for the liquid-phase epoxidation of olefins.[15–19]

Herein we report the preparation of the complex $[\{(\eta^5\text{-Ind})Mo(CO)_2(\mu\text{-Cl})\}_2]$ (**1**) and its use in the catalytic isomerisation of PinOx. Attention has been drawn to the identification of the metal species formed from **1** under different reaction conditions.

[a] Department of Chemistry, CICECO, University of Aveiro, Campus Universitário de Santiago, 3810-193 Aveiro, Portugal. E-mail: atav@ua.pt, igoncalves@ua.pt
[b] Instituto de Tecnologia Química e Biológica da Universidade Nova de Lisboa, Av. da República, Estação Agronómica Nacional, 2780-157 Oeiras, Portugal
[c] Escola Superior de Tecnologia, Instituto Politécnico de Setúbal, 2910-761 Setúbal, Portugal
[d] Centro de Química Estrutural, Complexo Interdisciplinar, Instituto Superior Técnico, Universidade de Lisboa, 1049-001 Lisbon, Portugal

† CCDC 980993. For crystallographic data in CIF or other electronic format see DOI: 10.1039/c4nj00371c

Experimental

Materials and methods

Microanalyses (CHN) were carried out at the University of Aveiro by M. Marques using a Truspec instrument. FT-IR spectra were recorded using a Bruker Tensor 27 spectrophotometer in a 4000–350 cm^{-1} range with 256 scans and 4 cm^{-1} resolution. Attenuated total reflectance (ATR) FT-IR spectra were recorded on the same instrument equipped with a Specac Golden Gate Mk II ATR accessory having a diamond top-plate and KRS-5 focussing lenses. FT-Raman spectra were recorded on a Bruker RFS 100 spectrometer with a Nd:YAG coherent laser (λ = 1064 nm). Solid-state magic-angle-spinning (MAS) ^{13}C NMR spectra were recorded at 100 MHz on a Bruker Avance 400 spectrometer with 3 μs ^{1}H 90° pulses, 2 ms contact time, a spinning rate of 10 kHz and 3 s recycle delays. Chemical shifts are quoted in parts per million from tetramethylsilane.

ESI mass spectra were obtained on a 500-MS quadrupole ion trap mass spectrometer (Varian Inc., Palo Alto, CA, USA). The sample was introduced into the ESI ion source using a syringe pump set to a flow rate of 20 μL min^{-1}. The ion spray voltage was set at ±5 kV; capillary voltage: 20–80 V and RF loading 90–80%. Nitrogen was used as nebulising and drying gas at pressures of 35 psi and 10 psi, respectively; drying gas temperature, 350 °C. The spectra were recorded in the range 100–1000 Da. Spectra typically correspond to the average of 20–35 scans. Theoretical isotope patterns were calculated using CHEMCALC.[20]

Air-sensitive operations were carried out by using standard Schlenk techniques under a nitrogen atmosphere. 1 M HCl in diethyl ether, pentane (99%), hexane (99%), 1,2-dichloroethane (DCE, 99%), anhydrous α,α,α-trifluorotoluene (TFT, >99%) and anhydrous acetonitrile (>99.8%) were purchased from Sigma-Aldrich. Where appropriate solvents were dried following standard procedures (THF, diethyl ether and hexane over Na/benzophenone ketyl; CH_2Cl_2 and DCE over CaH_2) and distilled under nitrogen. [(η^5-Ind)Mo(η^3-C_3H_5)$(CO)_2$] was prepared as previously reported.[21,22]

Synthesis of [{(η^5-Ind)Mo$(CO)_2$(μ-Cl)}$_2$] (1)

1 M HCl in diethyl ether (6.0 mL, 6.00 mmol) was added dropwise to a solution of [(η^5-Ind)Mo(η^3-C_3H_5)$(CO)_2$] (0.51 g, 1.67 mmol) in CH_2Cl_2 and the reaction mixture was stirred for 2 h at room temperature. The resultant red brown precipitate was filtered off, washed with diethyl ether and vacuum-dried. Yield: 0.49 g (98%). Anal. calcd for $C_{22}H_{14}Cl_2Mo_2O_4$ (605.13): C, 43.66; H, 2.33%. Found: C, 43.39; H, 2.32%. FT-IR (ATR, cm^{-1}): ν = 3097 (w), 2059 (w), 1954 (vs, ν(CO)), 1851 (vs, ν(CO)), 1602 (w), 1542 (m), 1477 (m), 1460 (m), 1376 (m), 1328 (m), 1240 (w), 1218 (w), 1153 (w), 1096 (w), 1039 (m), 984 (m), 902 (m), 832 (s), 745 (vs), 601 (m), 592 (m), 563 (m), 517 (m), 496 (m), 470 (w), 453 (m), 443 (s), 385 (w). FT-Raman (cm^{-1}): ν = 3095 (w), 3070 (w), 3049 (w), 1951 (w), 1842 (m), 1545 (w), 1447 (w), 1376 (w), 1328 (vs), 1240 (w), 1160 (w), 1038 (w), 1006 (w), 908 (w), 738 (w), 594 (w), 562 (w), 520 (w), 496 (m), 458 (w), 390 (m), 284 (m), 262 (w), 184 (w), 165 (s), 122 (vs), 106 (vs). ^{13}C CP MAS NMR: δ = 265.7 (CO), 259.2 (CO), 130.2 ($C^{8,9}$), 129.0 ($C^{5,6}$), 123.9 ($C^{4,7}$), 89.9 (C^{2}), 76.4 ($C^{1,3}$).

Single crystal X-ray diffraction

Single crystals of [(η^3-Ind)Mo$(CO)_2Cl(CH_3CN)_2$] (2) were manually harvested from the crystallisation vial and immediately immersed in highly viscous FOMBLIN Y perfluoropolyether vacuum oil (LVAC 140/13, Sigma-Aldrich) to avoid degradation caused by the evaporation of the solvent.[23] Crystals were mounted on Hampton Research CryoLoops with the help of a Stemi 2000 stereomicroscope equipped with Carl Zeiss lenses. Data were collected on a Bruker X8 Kappa APEX II CCD area-detector diffractometer (Mo Kα graphite-monochromated radiation, λ = 0.71073 Å) controlled using the APEX2 software package[24] and equipped with an Oxford Cryosystems Series 700 cryostream monitored remotely using the software interface Cryopad.[25] Images were processed using the software package SAINT+,[26] and data were corrected for absorption by the multiscan semi-empirical method implemented in SADABS.[27] The structure was solved using the Patterson synthesis algorithm implemented in SHELXS-97,[28] which allowed the immediate location of the crystallographically independent Mo^{II} centre and most of the heaviest atoms. The remaining non-hydrogen atoms were located from difference Fourier maps calculated from successive full-matrix least-squares refinement cycles on F^2 using SHELXL-97.[28a,29] All non-hydrogen atoms were successfully refined using anisotropic displacement parameters.

Hydrogen atoms bound to carbon were placed at their idealised positions using appropriate HFIX instructions in SHELXL: 133 for the methyl groups of the coordinated acetonitrile solvent molecules and 43 for the CH groups of the aromatic rings. All hydrogen atoms were included in subsequent refinement cycles with isotropic thermal displacement parameters (U_{iso}) fixed at 1.2 × U_{eq} (CH groups) or 1.5 × U_{eq} (methyl groups) of the parent carbon atoms.

The Flack parameter refined to −0.05(3).[30] The last difference Fourier map synthesis showed the highest peak (0.304 e $Å^{-3}$) located at 0.85 Å from C14 (one of the coordinated carbonyl groups) and the deepest hole (−0.355) at 0.23 Å from H1. Information concerning crystallographic data collection and structure refinement details is summarised in Table 1. Structural drawings were created using Crystal Impact Diamond.[31]

Catalytic tests

The catalytic reactions were carried out under air in a magnetically stirred, closed borosilicate reaction vessel (10 mL capacity) which was immersed in an oil bath thermostatted at 35 °C. Typically, the reactor was loaded with a metal complex (17 μmol of molybdenum), α-pinene oxide (PinOx, 170 μmol) and a solvent (0.5 mL). The PinOx was heated at the reaction temperature (10 min) prior to addition to a second heated reactor containing a solvent and a catalyst (instant taken as zero time). The course of the reaction was monitored using a Varian 3800 GC equipped with a BR-5 (Bruker) capillary column (30 m × 0.25 mm; 0.25 μm) and a flame ionisation detector, using H_2 as the carrier gas. Cyclododecane epoxide was used as an internal standard added after the reaction. The products were identified by GC-MS (Trace GC 2000 Series (Thermo Quest CE Instruments) – DSQ II (Thermo Scientific)), equipped with a capillary DB-5

Table 1 Crystal and structure refinement data for compound [(η^3-Ind)-Mo(CO)$_2$Cl(CH$_3$CN)$_2$] (**2**)

Formula	$C_{15}H_{13}ClMoN_2O_2$
Formula weight	384.66
Crystal system	Orthorhombic
Space group	$P2_12_12_1$
a/Å	8.0476(7)
b/Å	11.4511(10)
c/Å	16.8556(14)
Volume/Å^3	1553.3(2)
Z	4
D_c/g cm^{-3}	1.645
μ(Mo-Kα)/mm^{-1}	1.020
Crystal size/mm	0.07 × 0.05 × 0.02
Crystal type	Red blocks
θ range	3.56 to 29.13
Index ranges	$-10 \le h \le 11$, $-14 \le k \le 15$, $-23 \le l \le 22$
Reflections collected	30 905
Independent reflections	4143 [R_{int} = 0.0361]
Completeness to θ = 29.13°	99.7%
Final R indices [$I > 2\sigma(I)$][a,b]	R_1 = 0.0233, wR_2 = 0.0446
Final R indices (all data)[a,b]	R_1 = 0.0271, wR_2 = 0.0457
Weighting scheme[c]	m = 0.0215, n = 0.2428
Largest diff. peak and hole	0.304 and −0.355 e Å^{-3}

[a] $R_1 = \sum||F_o| - |F_c||/\sum|F_o|$. [b] $wR_2 = \sqrt{\sum\left[w(F_o^2 - F_c^2)^2\right]/\sum\left[w(F_o^2)^2\right]}$. [c] $w = 1/[\sigma^2(F_o^2) + (mP)^2 + nP]$ where $P = (F_o^2 + 2F_c^2)/3$.

type column (30 m × 0.25 mm; 0.25 μm) and using He as carrier gas.

Results and discussion

Catalyst preparation

The indenyl complex [{(η^5-Ind)Mo(CO)$_2$(μ-Cl)}$_2$] (**1**) was synthesised in nearly quantitative yield by reaction of [(η^5-Ind)Mo(η^3-C$_3$H$_5$)(CO)$_2$] with HCl (1 M in diethyl ether) in dichloromethane at room temperature. The method is particularly attractive since the allyl precursor is conveniently available from [Mo(η^3-C$_3$H$_5$)-Cl(CO)$_2$(CH$_3$CN)$_2$] and KInd in almost quantitative yield.[21] Recently, Honzíček *et al.* isolated dimeric **1** after bubbling gaseous HCl (Sigma-Aldrich) through a solution of [(η^5-Ind)Mo-(η^3-C$_3$H$_5$)(CO)$_2$].[32] Under similar reaction conditions, bubbling gaseous HCl (Air Liquide) through the solution at a high flow rate instead of HCl (1 M in diethyl ether) in a more controlled reaction produces [(η^5-Ind)Mo(CO)$_2$Cl$_3$] in excellent yield.[33] In the solid state, **1** is stable to air and moisture for several hours. The solid-state ^{13}C CP MAS NMR spectrum presents the indenyl signals with chemical shifts characteristic of the η^5-coordination mode, being similar to those observed for other pentahapto indenyl ligands in [(η^5-Ind)Mo{κ^2-S$_2$P(OEt)$_2$}-(CO)$_2$][34] and [(η^5-Ind)Mo(η^3-C$_3$H$_5$)(CO)$_2$].[35]

Catalytic isomerisation of α-pinene oxide

Complex **1** was investigated in the acid-catalysed isomerisation of α-pinene oxide (PinOx), using 1,2-dichloroethane (DCE) as a solvent. Outstandingly high catalytic activity was observed, leading to 100% conversion within 1 min of reaction at 55 °C, or within 30 min at approximately room temperature (35 °C, Table 2). Campholenic aldehyde (CPA) was the main product formed in *ca.* 68% selectivity at 100% conversion, in the reaction temperature range 35–55 °C (Scheme 1). Increasing the reaction time to 24 h did not lead to significant differences in product selectivity, suggesting that CPA is relatively stable under the reaction conditions used. Other products included the menthyl derivative *trans*-carveol (TCV), and the derivatives with a pinane skeleton, iso-pinocamphone (IPC) and *trans*-pinocarveol (PCV). The reaction did not take place to a measurable extent when carried out in the absence of a catalyst. These results are considerably superior to those reported recently by some of us for the first molybdenum-based homogeneous catalysts tested in the isomerisation of PinOx (Table 3).[13] The complexes [(η^5-Ind)Mo(η^3-C$_3$H$_5$)(CO)$_2$], [(η^5-IndCH$_3$)Mo(η^3-C$_3$H$_5$)(CO)$_2$] and [(η^5-IndSi(CH$_3$)$_3$)Mo(η^3-C$_3$H$_5$)(CO)$_2$] (IndCH$_3$ = C$_9$H$_6$CH$_3$; IndSi(CH$_3$)$_3$ = C$_9$H$_6$Si(CH$_3$)$_3$) led to 64%, 66% and 61% PinOx conversion, respectively, and CPA yields in the range of

Table 2 Isomerisation of α-pinene oxide in the presence of **1**[a]

Solvent	Temp. (°C)	Reaction time (min)	PinOx conv. (%)	CPA selectivity (%)
DCE	55	1	100	68
	35	1	90	58
	35	30	100	67
TFT	55	1	100	65
Hexane	55	1	20	53
	55	30	70	52
	55	60	100	54
CH$_3$CN	55	1	1	56
	55	300	94	52
	55	1440	100	53

[a] Reaction conditions: 17 μmol Mo, 170 μmol PinOx, 0.5 mL solvent.

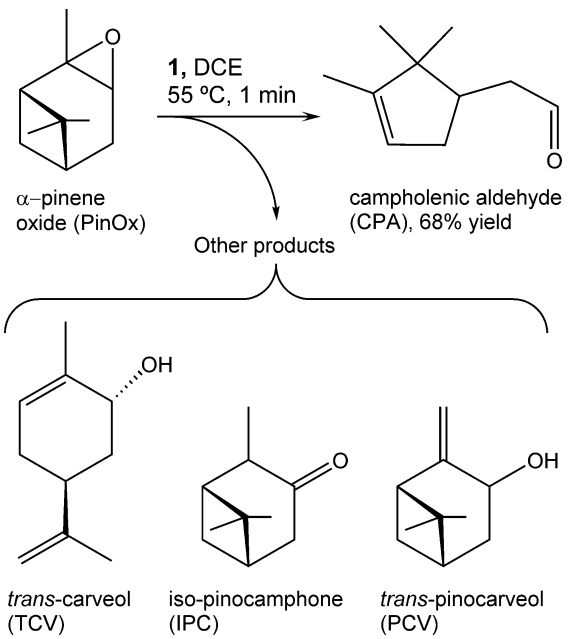

Scheme 1 Isomerisation of PinOx in the presence of **1**.

Table 3 Comparison of the catalytic results with **1** with those reported in the literature for molybdenum dicarbonyl complexes tested in the catalytic isomerisation of α-pinene oxide[a]

Catalyst	Time (min)	PinOx conv. (%)	CPA yield (%)	Other product yields (%)	Ref.
1	1	100	68	8-IPC 9-TCV	This work
$[(\eta^5\text{-Ind})Mo(\eta^3\text{-}C_3H_5)(CO)_2]$	60	64	33	12-TCV	13
$[(\eta^5\text{-Ind}CH_3)Mo(\eta^3\text{-}C_3H_5)(CO)_2]$	60	66	38	13-TCV	13
$[(\eta^5\text{-Ind}Si(CH_3)_3)Mo(\eta^3\text{-}C_3H_5)(CO)_2]$	60	61	33	12-TCV	13

[a] Reaction conditions: 17 μmol catalyst, 170 μmol PinOx, 0.5 mL DCE, 55 °C.

33–38%, at 1 h reaction, at 55 °C (a molar ratio of Mo/PinOx = 1 : 10, which is similar to that used in the present work, using DCE as a solvent).[13]

The catalytic results of **1** were similarly outstanding when using α,α,α-trifluorotoluene (TFT) as a solvent instead of DCE, at 55 °C (65% CPA selectivity at 100% conversion reached at 1 min reaction, Table 2). The relatively low toxicity and high boiling point (102 °C) of TFT make it a potentially interesting substitute for chlorinated solvents such as CH_2Cl_2 and DCE in organic reactions.[36] When hexane was used as a solvent, the reaction of PinOx was considerably slower (20% conversion at 1 min), and CPA selectivity was lower (54% CPA selectivity at 100% conversion). Using acetonitrile as a solvent led to a much slower reaction of PinOx isomerisation (1% conversion at 1 min), and CPA selectivity at 100% conversion was 53% (reached at 24 h reaction, Table 2). The initial reaction rates correlate with the dipole moments of the noncoordinating solvents which are higher for TFT and DCE (2.86 D and 1.36 D, respectively) than for hexane (0 D).[37] Possibly, the active species are more soluble in more polar solvents, leading to higher reaction rates. This correlation does not apply for the coordinating solvent CH_3CN (dipole moment of 3.95 D[37]), which gave the lowest reaction rate. The CH_3CN molecules are relatively basic which may level off the acidity of the metal species and consequently their activity in the target reaction. On the other hand, different metal species may be formed, which may be stabilised by the coordinating solvent molecules (ascertained by ESI-MS and single crystal X-ray diffraction studies, discussed below).

Characterisation studies

For DCE, TFT and hexane, the reaction mixtures were biphasic solid–liquid, while for CH_3CN only a residual amount of undissolved solid was observed. To get insights into the type of active species formed, the solid phases were separated from the reaction mixtures by centrifugation after 1 h reaction to give the solids denoted as DCE-s(cat), TFT-s(cat) and Hex-s(cat). A reaction time of 1 h was chosen partly because 100% conversion was reached at this point for all three solvents. Species dissolved in the corresponding liquid phases were precipitated by addition of pentane, which led to the solids denoted as DCE-l(cat), TFT-l(cat) and Hex-l(cat). All the solids obtained were washed with pentane–hexane, dried overnight at room temperature, and characterised by ATR FT-IR spectroscopy. While for DCE and TFT the solids recovered from the liquid and solid phases were blue-green in color, for hexane the solids were purple. For each solvent used, the species isolated from the solid and liquid phases exhibited similar FT-IR spectra (Fig. 1). However, for each type of solvent, considerable differences between the spectra of the recovered solids and that of **1** were observed. These results indicate that **1** is converted into different types of metal species under the reaction conditions used. While for DCE and TFT the complete disappearance (or nearly) of the bands characteristic of the carbonyl ligands was observed, these bands remained evident when hexane was used as a solvent. For DCE and TFT, the solids exhibited somewhat similar spectral features, whereas those for hexane exhibited a mixture of features between those of **1** and those of the solids recovered for the halogenated solvents. The similar spectra of the solids for DCE and TFT as solvents are consistent with the similar catalytic results obtained, and the similar colors of the

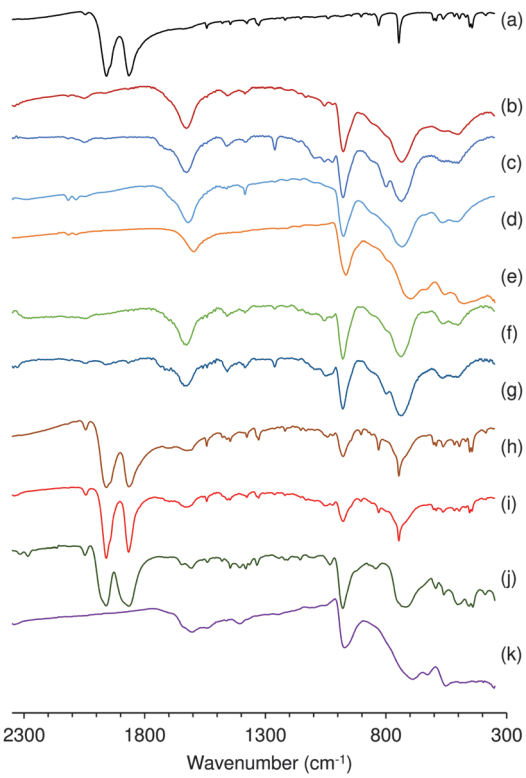

Fig. 1 FT-IR spectra of (a) compound **1**, and the recovered solids (b) DCE-s(cat), (c) DCE-l(cat), (d) DCE-s(55), (e) DCE-s(rt), (f) TFT-s(cat), (g) TFT-l(cat), (h) Hex-s(cat), (i) Hex-l(cat), (j) CH_3CN-s(55) and (k) CH_3CN-s(rt).

solids DCE-s(cat), DCE-l(cat), TFT-s(cat) and TFT-l(cat). On the other hand, the spectral differences between the solids obtained using the halogenated solvents and hexane are consistent with their different colors, and with the above hypothesis that the metal species are less soluble in hexane, leading to a lower overall reaction rate of PinOx. It is possible that **1** acts as a precatalyst, undergoing decarbonylation upon dissolution in the presence of air/water to give active species, and this reaction may be slower for hexane than for the halogenated solvents. For the three solvents, several new bands appeared, *e.g.* at *ca.* 1630, 975 and 735 cm^{-1}, which can be assigned to a water bending vibration, and stretching vibrations of Mo═O and Mo–O–Mo bonds, respectively.

In two further experiments carried out in the absence of PinOx, complex **1** was added to DCE (undried) and the mixture was stirred at either 55 °C for 1 h or room temperature for 24 h under air. The former experiment was carried out using the same quantities as those used in a typical catalytic test, while the latter experiment was carried out on a larger (*ca.* 10-fold increase) scale (0.05 g **1**, 83 μmol; 5 mL DCE). In each experiment a solid (0.02 g for the large-scale experiment) was recovered by filtration, washed with pentane and vacuum-dried. The FT-IR spectra of the solids (denoted DCE-s(55) and DCE-s(rt)) were quite similar to those recorded for the solids recovered after catalytic reactions performed in the presence of PinOx using either DCE or TFT as a solvent (Fig. 1).

To gain further insight into the possible nature of this compound, ESI studies were carried out for DCE-s(rt) in acetone. The negative ion ESI mass spectrum exhibited a group of peaks centered at *m*/*z* 440 with an isotopic pattern characteristic of a polynuclear Mo complex containing Cl, in particular a doubly charged tetranuclear complex. For example, the pattern agreed well with that calculated for $[Mo_4O_8Cl_4(H_2O)_6(C_3H_6O)_2]^{2-}$, where C_3H_6O = acetone. However, no plausible structure can be proposed for a compound having this formula. On the other hand, numerous compounds containing the tetranuclear $[Mo_4O_8(OR)_2(ROH)_2Cl_4]^{2-}$ (R = Me, Et) anionic unit are known, all comprising the rhombic $[Mo_4O_4(\mu_3\text{-}O)_2(\mu_2\text{-}O)_2(\mu_2\text{-}OR)_2]^{2+}$ core (Fig. 2).[38] This rhomboid disposition of metal atoms is a frequently encountered structural motif in molybdenum(v) coordination chemistry, appearing, for example, in the hydroxyl-bridged derivatives $[Mo_4O_8(OH)_2(Hpz^{Me2})_6]I_2$ (Hpz^{Me2} = 3,5-dimethylpyrazole)[39] and $K_2[Mo_4O_8(OH)_2(H_2O)_2(C_2O_4)_2]$,[40] and the Mo^V–glycolate complex $(PyH)_4[Mo_4O_8Cl_4(glyc)_2]$ (Py = pyridine).[41] In the FT-IR spectra of these compounds, strong bands are usually present at 950–980 for ν(Mo═O) and 660–760 cm^{-1} for ν(Mo–O–Mo), similar to those observed in this work for the recovered solids. The rhombic tetranuclear core may be regarded as a fusion of two $\{Mo_2O_4\}^{2+}$ units sharing a pair of triply-bridging oxo groups and a pair of doubly-bridging OR groups. The overall charge of the complex is then dependent on the nature of the 6 remaining peripheral ligands (*e.g.*, 2 L and 4 Cl in Fig. 2). In recent work we found that aerial oxidation of **1** in DMF gave the dinuclear oxomolybdenum(v) chloride $[Mo_2O_2(DMF)_4(\mu\text{-}O)_2Cl_2]$ containing the same type of $\{Mo_2O_4\}^{2+}$ unit found in the tetranuclear complexes described above.[42] Hence it seems plausible that a tetranuclear oxomolybdenum(v) complex could be a species formed from **1** under the catalytic reaction conditions used.

As mentioned above, when acetonitrile was used as a solvent in the catalytic reaction, only a residual amount of undissolved solid was observed. To gain insight into the stability of **1** in this solvent, the following additional experiments were performed in the absence of PinOx: (I) in a manner similar to that carried out for DCE-s(55) and DCE-s(rt), **1** (0.05 g, 83 μmol) and acetonitrile (5 mL) were stirred together for either 1 h at 55 °C or 48 h at room temperature, and the resultant suspended solid was recovered by filtration, washed with pentane and vacuum-dried, giving CH_3CN-s(55) and CH_3CN-s(rt); (II) compound **1** (0.1 g, 0.17 mmol) was dissolved in dry acetonitrile (5 mL) and the solution was immediately filtered and evaporated to dryness, giving a brown solid, which was washed with dry hexane (2 × 10 mL) and diethyl ether (2 × 10 mL), and finally vacuum-dried; (III) **1** was dissolved in dry MeCN and the solution was immediately analysed by ESI mass spectrometry.

The FT-IR spectrum of CH_3CN-s(rt) was very similar to that of DCE-s(rt) (Fig. 1), indicating that in the presence of air oxidative decarbonylation of **1** takes place upon dissolution to give the same type of oxomolybdenum species. In the case of CH_3CN-s(55), the solid presented a spectrum similar to those recorded for Hex-l(cat) and Hex-s(cat), *i.e.*, indicative of a mixture of species including unreacted **1**. These results may partly explain the poor initial catalytic activity observed when using CH_3CN as a solvent, at 55 °C.

Recrystallisation of the brown solid obtained in experiment II by slow diffusion of diethyl ether into a concentrated solution of the compound in dry acetonitrile under nitrogen gave red crystals, which were identified by X-ray diffraction as the ring-slipped dicarbonyl complex $[(\eta^3\text{-Ind})Mo(CO)_2Cl(CH_3CN)_2]$ (**2**) (Scheme 2; please see below for a full structural description).

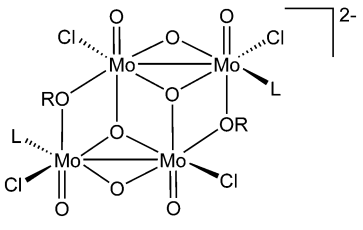

Fig. 2 Schematic representation of the rhombic $[Mo^V_4O_4(\mu_3\text{-}O)_2(\mu_2\text{-}O)_2(\mu_2\text{-}OR)_2(L)_2Cl_4]^{2-}$ anion.

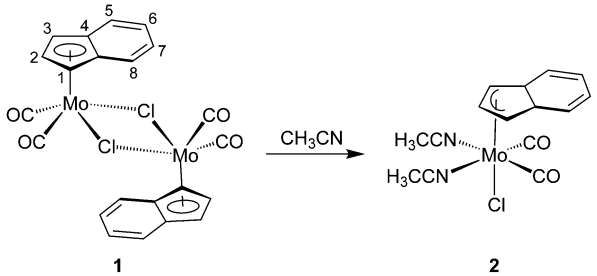

Scheme 2 Formation of **2** after dissolution of **1** in dry CH_3CN.

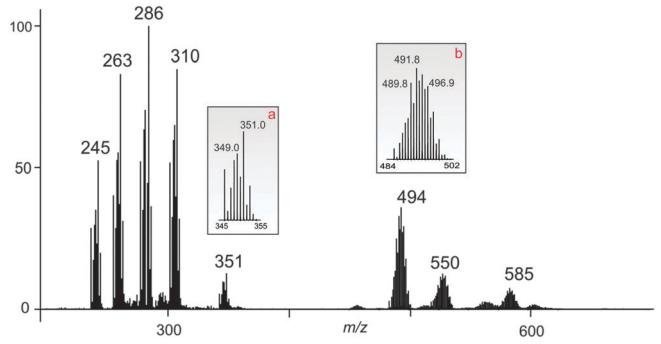

Fig. 3 Positive mode ESI spectrum of **1** in dry CH_3CN. Insets (a) and (b) illustrate the calculated isotopic distributions for the species $[IndMo(CO)_2(CH_3CN)_2]^+$ and $[(Ind)_2Mo_2Cl_2]^+$, respectively.

These results somewhat support the above hypothesis of the conversion of **1** to different metal species which may be stabilised by the CH_3CN (base) molecules. Nevertheless, on the basis of the FT-IR studies, complex **1** is also converted to other metal species which are possibly common to the different solvents tested.

The positive mode ESI spectrum recorded after infusion of a dry CH_3CN solution of **1** exhibited two major isotopic patterns, corresponding to mono- and dinuclear species, respectively. The mononuclear region showed a group of peaks at *m*/*z* 351 and 310 each of which displayed a seven-peak isotopic pattern characteristic of a single Mo atom that agreed well with that calculated for $[IndMo(CO)_2(CH_3CN)_2]^+$ (Fig. 3, inset a) and $[IndMo(CO)_2(CH_3CN)]^+$, respectively. The major patterns at *m*/*z* 230–290 correspond to adduct species formed in the gas-phase due to the presence of residual methanol and water molecules. Two groups of major peaks appear in the dimolybdenum region, fitting the calculated isotopic distributions for species containing two Mo centers and two Cl atoms (Fig. 3, inset b). The presence of these species was confirmed by MS/MS analysis. The most abundant species are listed in Table 4.

The negative mode ESI spectrum recorded immediately after infusion of a dry CH_3CN solution of **1** displayed two peaks

Table 4 Molybdenum species observed in the positive mode ESI mass spectrum of **1** (solvent = CH_3CN)

m/*z*[a]	Calculated monoisotopic mass	Probable species
245	244.98	$[(C_9H_7)Mo(CH_3OH)]^+$
263	262.99	$[(C_9H_7)Mo(H_2O)(CH_3OH)]^+$
286	286.01	$[(C_9H_7)Mo(CH_3CN)(CH_3OH)]^+$
310	309.97	$[(C_9H_7)Mo(CO)_2(CH_3CN)]^+$
351	351.00	$[(C_9H_7)Mo(CO)_2(CH_3CN)_2]^+$
457/459	460.88	$[(C_9H_7)_2Mo_2Cl]^+$
492/494	495.86	$[(C_9H_7)_2Mo_2Cl_2]^+$
527/529	530.83	$[(C_9H_7)_2Mo_2Cl_3]^+$
548/550	551.84	$[(C_9H_7)_2Mo_2Cl_2(CO)_2]^+$
564/566	565.79	$[(C_9H_7)_2Mo_2Cl_4]^+$
583/585	586.81	$[(C_9H_7)_2Mo_2Cl_3(CO)_2]^+$
604/606	607.83	$[(C_9H_7)_2Mo_2Cl_2(CO)_4]^+$

[a] More abundant peaks in the envelope isotope patterns. Species were assigned based on matches between calculated and observed isotopic patterns.

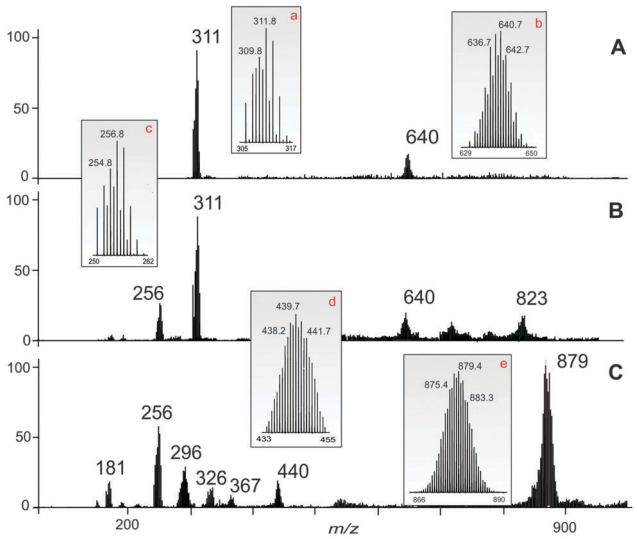

Fig. 4 Negative mode ESI spectra of **1** in dry CH_3CN at different infusion times: (A) immediately after infusion; (B) after 2 min; (C) after 10 min. Insets: calculated isotopic patterns matching the main species. In inset d, the isotopic separation of 0.5 *m*/*z* units is indicative of a doubly charged ion.

Table 5 Molybdenum species observed in the negative mode ESI mass spectrum of **1** (solvent = CH_3CN)

m/*z*[a]	Calculated monoisotopic mass	Probable species
181	180.89	$[MoCl(CH_3O)(OH)]^-$
256	255.83	$[MoCl_3(H_2O)_2(OH)]^-$
311	310.81	$[MoCl_3(CO)_2(H_2O)(OH)_2]^-$
295	294.82	$[Mo_2Cl_8(CH_3CN)_2CH_3OH]^{2-}$
326	327.26	$[Mo_3Cl_8(CH_3OH)_2(OH)]^{2-}$
367	367.23	$[Mo_3Cl_{10}(CH_3CN)(CH_3OH)(H_2O)]^{2-}$
440	440.67	$[Mo_4Cl_{11}(CH_3CN)(CH_3OH)_2]^{2-}$
638/640	639.68	$[Mo_2Cl_6(CO)_4(CH_3CN)(CH_3OH)_2(OH)]^-$
821/823	825.30	$[Mo_4Cl_{11}(CH_3OH)(OH)]^-$
877/879	881.35	$[Mo_4Cl_{11}(CH_3CN)(CH_3OH)_2]^-$

[a] See footnote *a* in Table 4.

centered at *m*/*z* 310.8 and 637.7/639.7, corresponding to $[MoCl_3(CO)_2(H_2O)(OH)_2]^-$ and $[Mo_2Cl_6(CO)_4(CH_3CN)(CH_3OH)_2(OH)]^-$, respectively (Fig. 4A). These species were not stable under the MS conditions used, and an oxidation process rapidly occurred leading to $[MoCl_3(H_2O)_2(OH)]^-$ with *m*/*z* 256 and loss of CO_2 (Fig. 4B). After 10 minutes of infusion, the mass spectrum (Fig. 4C) exhibited a substantial amount of mono- and doubly charged molybdenum species, indicating that rearrangement processes occurred in the gas-phase. The most abundant species are listed in Table 5.

Crystal structure of $[(\eta^3\text{-Ind})Mo(CO)_2Cl(CH_3CN)_2]$ (2)

Compound **2** crystallises in the non-centrosymmetric orthorhombic space group $P2_12_12_1$ with the asymmetric unit being composed of a whole $[(\eta^3\text{-Ind})Mo(CO)_2Cl(CH_3CN)_2]$ molecular unit (Fig. 5). The crystallographically independent Mo^{II} metal center is coordinated to an indenyl ligand, a chloride anion, two carbonyl groups and two acetonitrile solvent molecules,

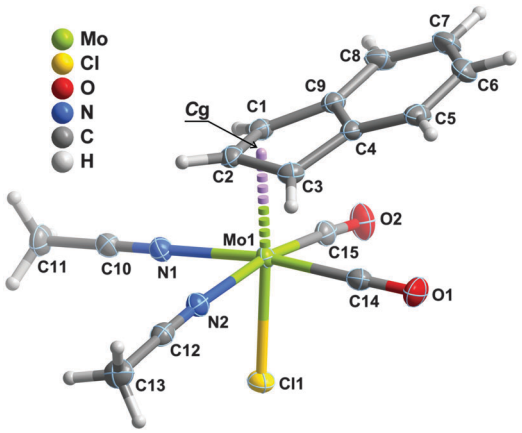

Fig. 5 Schematic representation of the asymmetric unit of **2**. Non-hydrogen atoms are represented as thermal ellipsoids drawn at the 50% probability level, and hydrogen atoms as small spheres with arbitrary radii. C_g stands for the centroid of the coordinating C1–C2–C3 atoms of the η^3-indenyl ligand. For selected bond lengths and angle ranges referring to the Mo^{II} coordination sphere see Table 6.

Table 6 Bond distances (in Å) and angles (in degrees) for the crystallographically independent Mo^{II} metal center present in **2**

Mo1–C14	1.968(2)	Mo1–C1	2.4101(19)
Mo1–C15	1.962(2)	Mo1–C2	2.1865(19)
Mo1–Cl1	2.4687(6)	Mo1–C3	2.393(2)
Mo1–N1	2.2283(16)	Mo1–$C_{g_{C1-C2-C3}}$	2.102(3)
Mo1–N2	2.2276(18)		
C1–Mo1–Cl1	153.00(5)	C15–Mo1–C2	107.28(8)
C2–Mo1–C1	35.54(7)	C15–Mo1–C3	108.06(8)
C2–Mo1–C3	35.93(8)	C15–Mo1–C14	81.20(8)
C2–Mo1–Cl1	160.20(6)	C15–Mo1–Cl1	88.27(6)
C2–Mo1–N1	83.39(7)	C15–Mo1–N1	96.73(7)
C2–Mo1–N2	83.10(7)	C15–Mo1–N2	169.41(8)
C3–Mo1–C1	56.38(7)	C15–Mo1–$C_{g_{C1-C2-C3}}$	96.00(11)
C3–Mo1–Cl1	150.30(5)	N1–Mo1–C1	81.24(6)
C14–Mo1–C1	106.74(7)	N1–Mo1–C3	118.47(7)
C14–Mo1–C2	106.09(8)	N1–Mo1–Cl1	82.63(5)
C14–Mo1–C3	70.85(8)	N1–Mo1–$C_{g_{C1-C2-C3}}$	94.75(10)
C14–Mo1–Cl1	88.02(6)	N2–Mo1–C1	117.68(6)
C14–Mo1–N1	170.50(8)	N2–Mo1–C3	81.50(7)
C14–Mo1–N2	98.18(7)	N2–Mo1–Cl1	81.14(5)
C14–Mo1–$C_{g_{C1-C2-C3}}$	94.68(11)	N2–Mo1–N1	82.14(6)
C15–Mo1–C1	72.34(8)	N2–Mo1–$C_{g_{C1-C2-C3}}$	94.59(10)
		Cl1–Mo1–$C_{g_{C1-C2-C3}}$	175.24(9)

with each pair of identical ligands being *cis* to each other within the coordination polyhedron of the metal center.

A search in the literature and in the Cambridge Structural Database (CSD, Version 5.34, November 2012 with 3 updates)[43] reveals that this organometallic complex is very unique among molybdenum complexes bearing derivatives of indenyl molecules and coordinated to halogen anions. Indeed, partial structural resemblances can solely be found in the complexes reported by Mawby & Pringle[44] and Schumann *et al.*[45] bearing indenyl and 2-menthylindenyl ligands, respectively. Nevertheless, in these two already known structures the metal center has a strikingly distinct coordination environment from that found in **2** (see below): they resemble a four-legged piano stool with an overall coordination number of five.

The most striking feature of the $[(\eta^3\text{-Ind})Mo(CO)_2Cl(CH_3CN)_2]$ complex is the presence of the indenyl group which, as shown in Fig. 5, loses planarity upon coordination to the metal center. The Hinge Angle (HA), the Fold Angle (FA) and the slip parameter (Δ) are numerical values that can be determined from the crystallographic data of **2** that ultimately permit an unequivocal characterisation of the coordination mode of the indenyl ligand to the Mo^{II} metal center and the determination of the hapticity of the ligand:[46]

$$\Delta = \overline{d[\mathrm{Mo}-(\mathrm{C4},\mathrm{C9})]} - \overline{d[\mathrm{Mo}-(\mathrm{C1},\mathrm{C3})]} \quad (1)$$

$$\mathrm{HA} = \angle[(\mathrm{C1},\ \mathrm{C2},\ \mathrm{C3}),\ (\mathrm{C1},\ \mathrm{C3},\ \mathrm{C4},\ \mathrm{C9})] \quad (2)$$

$$\mathrm{FA} = \angle[(\mathrm{C1},\ \mathrm{C2},\ \mathrm{C3}),\ (\mathrm{C4},\ \mathrm{C5},\ \mathrm{C6},\ \mathrm{C7},\ \mathrm{C8},\ \mathrm{C9})] \quad (3)$$

From the crystallographic determination the values are calculated as HA = 22.9(2)°, FA = 23.03(19)° and Δ = 0.753 Å, which is a clear indication of the η^3 hapticity of the indenyl ligand (coordinated *via* the C1, C2 and C3 atoms, Fig. 5).

Considering the centroid of the η^3-indenyl ligand as a single coordination site (as depicted in Fig. 5), the coordination environment around the metal center is best envisaged as a slightly distorted octahedron in which the apical positions are occupied by the charged ligands (the η^3-indenyl and the chloride anion) and the equatorial plane is composed of the neutral ones: while the internal octahedral distances cover the wide range from 1.962(2) to 2.4687(6) Å, the *cis* and *trans* octahedral angles are found in the narrow ranges of 81.14(5)–98.18(7) and 169.41(8)–175.24(9)°, respectively (Table 6). To further help in the evaluation of the variation of the degree of distortion of the Mo^{II} octahedron, an adaptation of a simple method proposed by Baur[47] to calculate a distortion index (DI) for bonds and angles can be employed:

$$\mathrm{DI}_{\mathrm{Bond}} = \frac{\sum_{i=1}^{n}\left|d(\mathrm{Mo}-\mathrm{L})_i - d(\mathrm{Mo}-\mathrm{L})_{\mathrm{average}}\right|}{\sum_{i=1}^{n}\left|d(\mathrm{Mo}-\mathrm{L})_i\right|} \quad (4)$$

$$\mathrm{DI}_{\mathrm{Angle}} = \frac{\sum_{i=1}^{n}\left|\angle(\mathrm{L}-\mathrm{Mo}-\mathrm{L})_i - \angle(\mathrm{L}-\mathrm{Mo}-\mathrm{L})_{\mathrm{ideal}}\right|}{\sum_{i=1}^{n}\left|\angle(\mathrm{L}-\mathrm{Mo}-\mathrm{L})_i\right|} \quad (5)$$

where L corresponds to any coordination site, and subscripts *i* and average/ideal indicate individual and average/ideal bond lengths and angles (see Table 6 for tabulated data). For an octahedron the value of $\mathrm{DI}_{\mathrm{Angle}}$ should be calculated independently of the *cis* and *trans* angles, and always compared to the ideal values (*i.e.*, 90 and 180°, respectively). In this way, the $\mathrm{DI}_{\mathrm{Bond}}$ value is calculated as 0.069, while the $\mathrm{DI}_{\mathrm{Angle}}$ parameters for the *cis* and *trans* angles are 0.066 and 0.028. These values unequivocally indicate that the dispersion of bond lengths and *cis* octahedral angles is at the genesis of the distortion of the octahedral coordination environment. This was expected *a priori* due to the very distinct chemical nature of the various ligands. These studies further show that despite the bulky

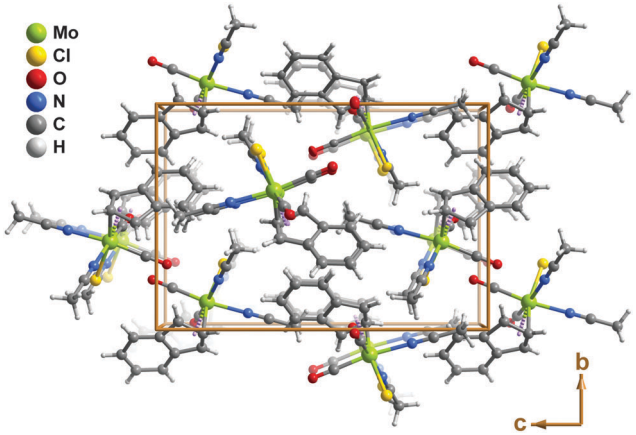

Fig. 6 Crystal packing of [(η^3-Ind)Mo(CO)$_2$Cl(CH$_3$CN)$_2$] (**2**) viewed in perspective along the [100] direction of the unit cell. Supramolecular contacts have been omitted for clarity.

Table 7 Supramolecular contacts present in [(η^3-Ind)Mo(CO)$_2$Cl(CH$_3$CN)$_2$] (**2**)[a,b]

D–H···A	d(D···A) (Å)	<(DHA) (degrees)
C13–H13B···Cl1^{i}	3.461(2)	164
C–H···π contacts	**d(C···π) (Å)**	**<(CHπ) (degrees)**
C8–H8···C_{g1}^{ii}	3.811(3)	149

[a] Symmetry transformations used to generate equivalent atoms: (i) $-1+x, y, z$; (ii) $1/2+x, 1.5-y, 1-z$. [b] Centroids (C_g) (see Fig. 5): C_{g1} = C4, C5, C6, C7, C8 and C9.

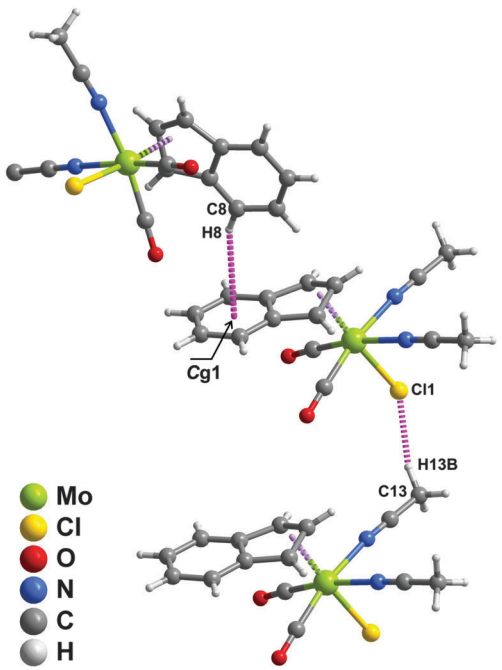

Fig. 7 Supramolecular arrangement of individual [(η^3-Ind)Mo(CO)$_2$Cl(CH$_3$CN)$_2$] molecular units in the crystal packing of compound **2**. Interactions are based on weak C–H···Cl and C–H···π contacts (purple green lines). C_{g1} stands for the centroid of the six-membered aromatic ring of the indenyl group. For geometrical details on the represented supramolecular contacts see Table 7. Symmetry transformations used to generate equivalent atoms have been omitted for clarity.

nature of some of the ligands, the overall coordination polyhedron permits their accommodation around the metal center, leading to near-to-ideal *trans* angles (as clearly indicated by the very low DI$_{Angle}$ parameter for the *trans* angles).

Individual [(η^3-Ind)Mo(CO)$_2$Cl(CH$_3$CN)$_2$] complexes closely pack in the solid state to yield the crystal structure of compound **2** (Fig. 6) mediated, on the one hand, by the need to effectively fill the available space and, on the other hand, by a small number of weak supramolecular contacts, namely C–H···Cl and C–H···π interactions (see Table 7 for specific geometrical data and Fig. 7 for a schematic representation of the interactions).

On the basis of these structural features, the dissolution of compound **1** in CH$_3$CN may be accompanied by the formation of soluble compounds of type **2**. On the other hand, the (non-coordinating) halogenated solvents possibly facilitate the solvation of **1** by disrupting relatively weak supramolecular interactions (accounting for faster overall catalytic reaction). In contrast to that observed for CH$_3$CN as a solvent, no traces of **1** were observed for DCE after 1 h at 55 °C (spectra j and d of Fig. 1, respectively).

Conclusion

We have shown that the organometallic complex [{(η^5-Ind)-Mo(CO)$_2$(μ-Cl)}$_2$] can be used for the catalytic isomerisation of α-pinene oxide to campholenic aldehyde, giving the desired product in good yield. The catalytic performance surpasses that previously found for related complexes of the type [(IndR)Mo-(η^3-C$_3$H$_5$)(CO)$_2$]. Under the reaction conditions used, the organometallic complex may function as a precatalyst, undergoing decarbonylation in the presence of air/water to give active species (in a manner comparable to that already extensively investigated for molybdenum carbonyl complexes used as catalyst precursors for the epoxidation of olefins). On the basis of a comparison of these results with those previously described for transition-metal-based homogeneous catalysts, further exploration of organomolybdenum complexes as (pre)catalysts for this industrially relevant reaction is warranted.

Acknowledgements

This work was partly financed by FEDER (Fundo Europeu de Desenvolvimento Regional) through COMPETE (Programa Operacional Factores de Competitividade) and by national funds through the FCT (Fundação para a Ciência e a Tecnologia) with the projects CICECO – FCOMP-01-0124-FEDER-037271 (FCT ref. PEst-C/CTM/LA0011/2013), FCOMP-01-0124-FEDER-029779 (FCT ref. PTDC/QEQ-SUP/1906/2012, including the research grant with ref. BPD/UI89/4864/2013 to A.C.G), the Centro de Química Estrutural (PEst-OE/QUI/UI0100/2013), and REM 2013. The FCT and the European Union are acknowledged for a post-doctoral grant to S.M.B. (ref. SFRH/BPD/46473/2008) cofunded by MCTES and the European Social Fund through the program POPH of QREN. We further wish to thank the FCT for specific funding towards the purchase of the single-crystal diffractometer. The NMR spectrometers used are part of

The National NMR Network (REDE/1517/RMN/2005), supported by POCI 2010 and the FCT. The authors thank the Portuguese NMR Network (IST-UTL Center) (RECI/QEQ-QIN/0189/2012) for providing access to the NMR facilities.

Notes and references

1 W. Schwab, C. Fuchs and F.-C. Huang, *Eur. J. Lipid Sci. Technol.*, 2013, **115**, 3.
2 V. V. Costa, K. A. da Silva Rocha, L. F. de Sousa, P. A. Robles-Dutenhefner and E. V. Gusevskaya, *J. Mol. Catal. A: Chem.*, 2011, **345**, 69.
3 I. V. Il'ina, K. P. Volcho and N. F. Salakhutdinov, *Russ. J. Org. Chem.*, 2008, **44**, 1.
4 K. A. da Silva Rocha, J. L. Hoehne and E. V. Gusevskaya, *Chem. – Eur. J.*, 2008, **14**, 6166.
5 K. A. da Silva Rocha, I. V. Kozhevnikov and E. V. Gusevskaya, *Appl. Catal., A*, 2005, **294**, 106.
6 G. Neri, G. Rizzo, A. Pistone, L. De Luca, A. Donato, M. G. Musolino and R. Pietropaolo, *Appl. Catal., A*, 2007, **325**, 25.
7 W. F. Hölderich, J. Röseler, G. Heitmann and A. T. Liebens, *Catal. Today*, 1997, **37**, 353.
8 C. Brocke, M. Eh and A. Finke, *Chem. Biodiversity*, 2008, **5**, 1000.
9 J. Kaminska, M. A. Schwegler, A. J. Hoefnagel and H. van Bekkum, *Recl. Trav. Chim. Pays-Bas*, 1992, **111**, 432.
10 M. W. C. Robinson, K. S. Pillinger, I. Mabbett, D. A. Timms and A. E. Graham, *Tetrahedron*, 2010, **66**, 8377.
11 L. Alaerts, E. Séguin, H. Poelman, F. Thibault-Starzyk, P. A. Jacobs and D. E. De Vos, *Chem. – Eur. J.*, 2006, **12**, 7353.
12 A. Dhakshinamoorthy, M. Alvaro, H. Chevreau, P. Horcajada, T. Devic, C. Serre and H. Garcia, *Catal. Sci. Technol.*, 2012, **2**, 324.
13 S. M. Bruno, C. A. Gamelas, A. C. Gomes, A. A. Valente, M. Pillinger, C. C. Romão and I. S. Gonçalves, *Catal. Commun.*, 2012, **23**, 58.
14 C. A. Gamelas, N. A. G. Bandeira, C. C. L. Pereira, M. J. Calhorda, E. Herdtweck, M. Machuqueiro, C. C. Romão and L. F. Veiros, *Dalton Trans.*, 2011, **40**, 10513.
15 P. J. Fischer, M. C. Neary, L. Avena, K. P. Sullivan and K. C. Hackbarth, *Organometallics*, 2012, **31**, 2437.
16 P. M. Reis, C. A. Gamelas, J. A. Brito, N. Saffon, M. Gómez and B. Royo, *Eur. J. Inorg. Chem.*, 2011, 666.
17 P. Neves, C. C. L. Pereira, F. A. A. Paz, S. Gago, M. Pillinger, C. M. Silva, A. A. Valente, C. C. Romão and I. S. Gonçalves, *J. Organomet. Chem.*, 2010, **695**, 2311.
18 S. Li, C. W. Kee, K.-W. Huang, T. S. A. Hor and J. Zhao, *Organometallics*, 2010, **29**, 1924.
19 V. V. K. M. Kandepi, A. P. da Costa, E. Peris and B. Royo, *Organometallics*, 2009, **28**, 4544.
20 L. Patiny and A. Borel, *J. Chem. Inf. Model.*, 2013, **53**, 1223.
21 (*a*) J. R. Ascenso, C. G. de Azevedo, I. S. Gonçalves, E. Herdtweck, D. S. Moreno, C. C. Romão and J. Zühlke, *Organometallics*, 1994, **13**, 429; (*b*) J. R. Ascenso, C. G. de Azevedo, I. S. Gonçalves, E. Herdtweck, D. S. Moreno, M. Pessanha and C. C. Romão, *Organometallics*, 1995, **14**, 3901.
22 J. W. Faller, C.-C. Chen, M. J. Mattina and A. Jakubowski, *J. Organomet. Chem.*, 1973, **52**, 361.
23 T. Kottke and D. Stalke, *J. Appl. Crystallogr.*, 1993, **26**, 615.
24 *APEX2 Data Collection Software, Version 2.1-RC13*, Bruker AXS, Delft, The Netherlands, 2006.
25 *Cryopad, Remote monitoring and control, Version 1.451*, Oxford Cryosystems, Oxford, United Kingdom, 2006.
26 *SAINT+, Data Integration Engine, version 7.23a*, Bruker AXS, Madison, Wisconsin, USA, 1997–2005.
27 G. M. Sheldrick, *SADABS, version 2.01, Bruker/Siemens Area Detector Absorption Correction Program*, Bruker AXS, Madison, Wisconsin, USA, 1998.
28 (*a*) G. M. Sheldrick, *SHELXS-97, Program for Crystal Structure Solution*, University of Göttingen, 1997; (*b*) G. M. Sheldrick, *Acta Crystallogr., Sect. A: Found. Crystallogr.*, 2008, **64**, 112.
29 G. M. Sheldrick, *SHELXL-97, Program for Crystal Structure Refinement*, University of Göttingen, 1997.
30 (*a*) H. D. Flack, *Acta Crystallogr., Sect. A: Found. Crystallogr.*, 1983, **39**, 876; (*b*) H. D. Flack and G. Bernardinelli, *Acta Crystallogr., Sect. A: Found. Crystallogr.*, 1999, **55**, 908; (*c*) H. D. Flack and G. Bernardinelli, *J. Appl. Crystallogr.*, 2000, **33**, 1143.
31 K. Brandenburg, *DIAMOND, Version 3.2f.*, Crystal Impact GbR, Bonn, Germany, 1997–2010.
32 J. Honzíček, J. Vinklárek, M. Erben, J. Lodinský, L. Dostál and Z. Padělková, *Organometallics*, 2013, **32**, 3502.
33 M. G. B. Drew, V. Félix, I. S. Gonçalves, C. C. Romão and B. Royo, *Organometallics*, 1998, **17**, 5782.
34 M. J. Calhorda, C. A. Gamelas, I. S. Gonçalves, E. Herdtweck, C. C. Romão and L. F. Veiros, *Organometallics*, 1998, **17**, 2597.
35 S. S. Braga, I. S. Gonçalves, A. D. Lopes, M. Pillinger, J. Rocha, C. C. Romão and J. J. C. Teixeira-Dias, *J. Chem. Soc., Dalton Trans.*, 2000, 2964.
36 A. Ogawa and D. P. Curran, *J. Org. Chem.*, 1997, **62**, 450.
37 J. L. M. Abboud and R. Notario, *Pure Appl. Chem.*, 1999, **71**, 645.
38 (*a*) B. Modec, J. V. Brenčič and J. Zubieta, *J. Chem. Soc., Dalton Trans.*, 2002, 1500; (*b*) B. Modec and J. V. Brenčič, *Eur. J. Inorg. Chem.*, 2005, 1698; (*c*) M. F. Belicchi, G. G. Fava and C. Pelizzi, *J. Chem. Soc., Dalton Trans.*, 1983, 65; (*d*) H. Kang, S. Liu, S. N. Shaikh, T. Nicholson and J. Zubieta, *Inorg. Chem.*, 1989, **28**, 920.
39 M. Cano, J. A. Campo, J. V. Heras, E. Pinilla and A. Monge, *Polyhedron*, 1996, **15**, 1705.
40 L. Lisnard, P. Mialane, A. Dolbecq, J. Marrot and F. Sécheresse, *Inorg. Chem. Commun.*, 2003, **6**, 503.
41 B. Modec, D. Dolenc and M. Kasunič, *Inorg. Chem.*, 2008, **47**, 3625.
42 A. C. Gomes, C. A. Gamelas, J. A. Fernandes, F. A. A. Paz, P. Nunes, M. Pillinger, I. S. Gonçalves, C. C. Romão, M. Abrantes, submitted.
43 (*a*) F. H. Allen, *Acta Crystallogr., Sect. B: Struct. Sci.*, 2002, **58**, 380; (*b*) F. H. Allen and W. D. S. Motherwell, *Acta Crystallogr., Sect. B: Struct. Sci.*, 2002, **58**, 407.
44 A. Mawby and G. E. Pringle, *J. Inorg. Nucl. Chem.*, 1972, **34**, 525.
45 H. Schumann, O. Stenzel, S. Dechert, F. Girgsdies and R. L. Halterman, *Organometallics*, 2001, **20**, 5360.
46 (*a*) V. Cadierno, J. Díez, M. Pilar Gamasa, J. Gimeno and E. Lastra, *Coord. Chem. Rev.*, 1999, **193–195**, 147; (*b*) S. A. Westcott, A. K. Kakkar, G. Stringer, N. J. Taylor and T. B. Marder, *J. Organomet. Chem.*, 1990, **394**, 777.
47 W. H. Baur, *Acta Crystallogr., Sect. B: Struct. Sci.*, 1974, **30**, 1195.